# Brown adipose tissue dynamics in wild-type and UCP1-knockout mice: in vivo insights with magnetic resonance[s]

Kirsten Grimpo,[1,]* Maximilian N. Völker,[†] Eva N. Heppe,* Steve Braun,[†] Johannes T. Heverhagen,[§] and Gerhard Heldmaier*

Faculty of Biology, Department of Animal Physiology,* and Faculty of Medicine, Department of Diagnostic Radiology,[†] Philipps-Universität Marburg, 35043 Marburg, Germany; and Institute for Diagnostic, Interventional, and Paediatric Radiology,[§] University Hospital Inselspital, Bern, Switzerland

**Abstract** We used noninvasive magnetic resonance imaging (MRI) and magnetic resonance spectroscopy to compare interscapular brown adipose tissue (iBAT) of wild-type (WT) and uncoupling protein 1 (UCP1)-knockout mice lacking UCP1-mediated nonshivering thermogenesis (NST). Mice were sequentially acclimated to an ambient temperature of 30°C, 18°C, and 5°C. We detected a remodeling of iBAT and a decrease in its lipid content in all mice during cold exposure. Ratios of energy-rich phosphates (ATP/ADP, phosphocreatine/ATP) in iBAT were maintained stable during noradrenergic stimulation of thermogenesis in cold- and warm-adapted mice and no difference between the genotypes was observed. As free fatty acids (FFAs) serve as fuel for thermogenesis and activate UCP1 for uncoupling of oxidative phosphorylation, brown adipose tissue is considered to be a main acceptor and consumer of FFAs. We measured a major loss of FFAs from iBAT during noradrenergic stimulation of thermogenesis. This mobilization of FFAs was observed in iBAT of WT mice as well as in mice lacking UCP1. The high turnover and the release of FFAs from iBAT suggests an enhancement of lipid metabolism, which in itself contributes to the sympathetically activated NST and which is independent from uncoupled respiration mediated by UCP1. Our study demonstrates that MRI, besides its potential for visualizing and quantification of fat tissue, is a valuable tool for monitoring functional in vivo processes like lipid and phosphate metabolism during NST.—Grimpo, K., M. N. Völker, E. N. Heppe, S. Braun, J. T. Heverhagen, and G. Heldmaier. **Brown adipose tissue dynamics in wild-type and UCP1-knockout mice: in vivo insights with magnetic resonance.** *J. Lipid Res.* 2014. 55: 398–409.

**Supplementary key words** lipid metabolism • nonshivering thermogenesis • phosphorus spectroscopy • proton spectroscopy • ultra-high field • uncoupling protein 1

Brown adipose tissue (BAT) is a thermogenically active organ and its thermoregulatory function is crucial for body temperature maintenance of small eutherian mammals and newborns during periods of cold exposure. BAT thermogenesis is activated by the release of noradrenaline (NA) from sympathetic innervation. Uncoupling protein 1 (UCP1) in the inner mitochondrial membrane of the brown adipocytes uncouples the respiratory chain from ATP synthesis and thus energy is dissipated as heat (1–3). Prolonged cold exposure or a short photoperiod induces the recruitment of BAT (4–6). Brown adipocytes of cold-adapted mice, contain small and multilocular lipid vacuoles, which are rich in cytoplasm and have a high content of mitochondrial protein (7–9). This provides an enhanced thermogenic capacity during cold exposure, and BAT can be considered as the major site of adaptive nonshivering thermogenesis (NST) in rodents and other small mammals (4, 10–12).

The breakdown of lipids via lipoprotein lipase plays an important role during UCP1-mediated heat production (13). Free fatty acids (FFAs) directly activate UCP1 and feed the respiratory chain, i.e., FFAs are the major substrate for NST (14, 15). Therefore active BAT is considered as a main consumer of lipids and FFAs and its contribution to plasma clearance of administered triglycerides has been shown previously (16, 17). On the other hand a release of fatty acids during thermogenesis from BAT has been assumed, indicating a substrate supply to other tissues (18, 19). Sympathetic activation by cold exposure or injections of NA not only activate BAT but also stimulate sympathetic receptors in general, leading to an increase in heart rate, blood flow, and metabolic responses in other tissues. The contribution of these UCP1-independent processes to total NST remain unclear (20, 21).

---

---

Abbreviations: BAT, brown adipose tissue; iBAT, interscapular brown adipose tissue; MRS, magnetic resonance spectroscopy; NA, noradrenaline; NST, nonshivering thermogenesis; PCr, phosphocreatine; TE, echo time; TR, repetition time; UCP1, uncoupling protein 1.
[1]To whom correspondence should be addressed.
  e-mail: grimpok@biologie.uni-marburg.de
[s] The online version of this article (available at http://www.jlr.org) contains supplementary data in the form of three figures and two videos.

UCP1-knockout (KO) mice are well-suited for investigation of UCP1-independent thermogenesis as mitochondria of these mice are lacking the thermogenic potential of UCP1. Their brown adipocytes contain lager lipid vacuoles similar to white adipocytes (22). UCP1-KO mice raised at thermoneutrality cannot maintain their body temperature upon immediate exposure to 4°C, as one would expect from the lack of UCP1. Nevertheless, a stepwise reduction of ambient temperature improves their thermogenic capacity and they develop a presentable cold tolerance during cold adaption (23). For this reason it has been suggested that UCP1-deleted mice use alternative mechanisms of adaptive thermogenesis, such as an enhanced capacity for shivering thermogenesis or brown adipocyte-like cells in white adipose tissue with higher oxidative capacity (24–26).

We compared the role of BAT during NST in wild-type (WT) and UCP1-KO mice with the help of magnetic resonance imaging (MRI) and magnetic resonance spectroscopy (MRS). The higher water content and the abundance of iron-rich mitochondria in brown adipocytes allow differentiation between brown and white adipose tissue in vivo (27–29), and thermogenically active layers can be distinguished from thermogenically inactive BAT layers (30–32). Therefore, we acclimatized WT and UCP1-KO mice to warm or cold ambient temperatures. To analyze the metabolic activity of interscapular brown adipose tissue (iBAT) of anesthetized mice in vivo, we imaged its phenotype and measured changes in lipid composition and phosphate levels during NA-induced NST. Further, the metabolic rate of conscious mice was obtained after stimulation with NA using indirect calorimetry. These methods allowed us to differentiate the role of BAT in WT and UCP1-KO mice and to confirm the use of noninvasive MRI for investigation of functional in vivo processes.

## MATERIAL AND METHODS

### Mice and acclimation protocol

WT mice and UCP1-deleted littermates (genetic background C57Bl/6J) were derived from heterozygous breeding pairs in our colony at Philipps-Universität Marburg. The breeding colony was kept at 27°C ambient temperature. In the founder animals (originally provided by L. Kozak, Pennington Medical Research Centre, Baton Rouge, LA), the UCP1 gene had been inactivated by homologous recombination (33). Genotypes were identified using a PCR-based strategy (23) prior to the first measurements. Only male UCP1$^{+/+}$ (WT) and UCP1$^{-/-}$ (KO) mice were included in the experiments. The presence or absence of UCP1 protein in BAT of mice was verified post mortem by enhanced chemiluminescence (ECL) Western blot assay (34). The membranes were probed with a rabbit anti-UCP1 polyclonal antibody (1:30,000 dilution, 3046, Chemicon) followed by a goat anti-rabbit-IgG peroxidase-conjugated secondary antibody (1:10,000 dilution, Dako). The chemiluminescent signal was detected on X-ray film (Super RX, Fuji) using an ECL Plus Western blotting detection system (SRX-101A, Konika Minolta).

Throughout the experiments mice were housed individually in macrolon type II cages bedded with wood shavings and nesting material. Mice were fed ad libitum with standard chow diet (Ssniff 1534, Soest, Germany), had free access to water, and were kept at a 12:12 h light:dark cycle. To investigate mice adapted to different ambient temperatures, they were sequentially acclimated to ambient temperatures of 30°C, 18°C, and 5°C. Mice at an age of 3–6 months were transferred to 30°C for 3 weeks, afterwards acclimated to 18°C for 3 weeks, and finally to 5°C for a further 2 weeks. Even though UCP1-KO mice are cold sensitive, they can tolerate an ambient temperature of 5°C when using this stepwise acclimation protocol (24). Thermogenic properties were measured (metabolic rate, MRI, and MRS) at the end of each acclimation period. The experiments were performed in accordance with the German animal welfare act.

### MRI and MRS

All MRI and MRS experiments were performed with a 7 Tesla small animal MRI scanner equipped with a 290 mT/m gradient system (ClinScan, Bruker Biospin MRI GmbH, Ettlingen, Germany). Mice were anesthetized with an intraperitoneal injection of pentobarbital sodium at a dose of 75 mg/kg body weight (Narcoren, Merial GmbH, Hallbergmoos, Germany). A subcutaneous access was administered to facilitate a NA injection (1 mg NA/kg body weight) through a polyethylene tube system during magnetic resonance measurements without relocating the mice.

During the measurements, the body temperature of the mice was stabilized with a heating unit. Respiration rate and rectal body temperature were continuously monitored (small animal monitoring and gating system, SAInstruments, Stony Brook, NY).

BAT composition and changes in lipid content of 31 mice [WT (n = 16), UCP1-KO (n = 15)] were examined using a quadrature mouse birdcage coil with an inner diameter of 35 mm (Bruker). To localize the iBAT depot and to differentiate it from other tissues, two imaging sequences were optimized in contrast parameters as follows (**Fig. 1A, B**): a T2-weighted turbo spin echo sequence [repetition time (TR), 1,010 ms; echo time (TE), 52 ms; FoV, 30 × 30 mm$^2$; matrix, 192 × 192; slices, 16; slice thickness, 0.8 mm; voxel size, 0.156 × 0.156 × 0.8 mm$^3$; acquisition time, 111 s] and a T1-weighted turbo spin echo sequence (TR, 478 ms; TE, 7.8 ms; matrix size, 256 × 256; slices, 16; slice thickness, 0.8 mm; voxel size, 0.117 × 0.117 × 0.8 mm$^3$; acquisition time, 94 s). Spectroscopic data were acquired with a point resolved spectroscopy sequence without water suppression (PRESS $^1$H-spectroscopy; TR, 2,500 ms; TE, 28 ms; flip angle, 90°; voxel size, 1.0 × 3.1 × 1.0 mm$^3$; 128 averages; acquisition time, 335 s). The measurement volume was set within the iBAT depot (Fig. 1 C inset). For each individual mouse five spectra were acquired, one spectrum before subcutaneous NA injection and four consecutive spectra with an overall time span of 22 min (after injection).

Twelve mice [WT (n = 5), UCP1-KO (n= 7)] were subjected to $^{31}$P-spectroscopic examination for energy-rich phosphates. For these measurements, a custom transmit/receive surface coil (16 × 16 mm in diameter) that was tuned to phosphorus Larmor frequency at 7 T (121.62 MHz) was built in-house (supplementary Fig. I). The coil was mounted on a curved tube section (20 × 40 mm) to ensure an optimal placement on the mouse's neck. The phosphorus spectroscopy was acquired using a free induction decay sequence (TR, 450 ms; 1,024 averages; flip angle, 50°; acquisition time, 461 s), i.e., an unlocalized sequence, which presupposes a precise coil localization on the interscapular region to obtain specific data of the BAT. The correct placement of the $^{31}$P-coil on the interscapular region (the coil was marked with an adalat capsule, see Fig. 1 D inset) and the localization of the target volume for spectroscopy were controlled with sagittal, coronal, and transversal $^1$H-imaging sequences via the integrated body coil insert of the tomograph. Adjustments of the MRI scanner were controlled manually and optimized in a 9.0 × 3.0 ×
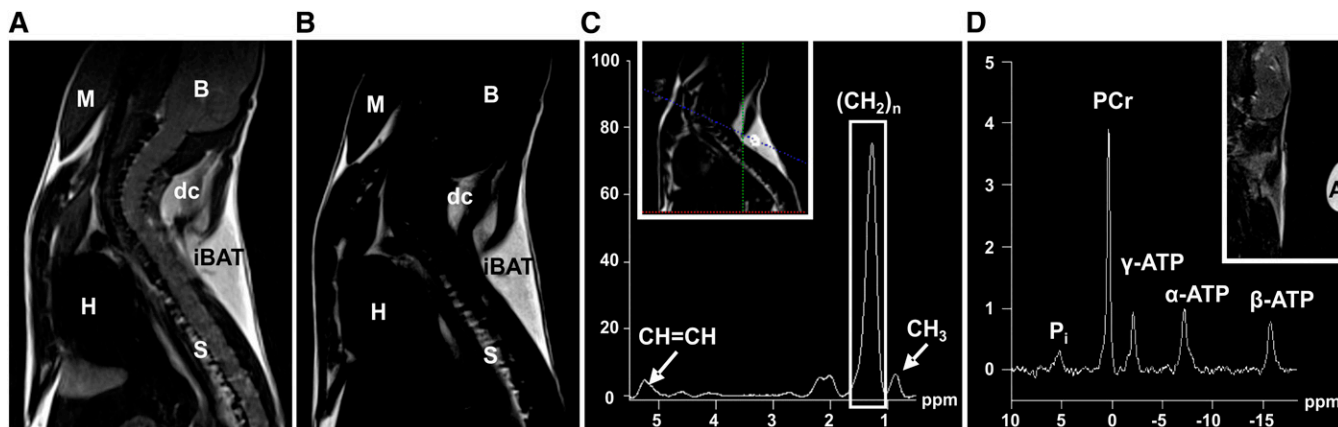
**Fig. 1.** Representative MRI and MRS acquired from the neck area of WT mice acclimated to 18°C ambient temperature. Overview of the neck area using a T2-weighted imaging sequence (A) and a T1-weighted sequence with water suppression (B). B, brain; M, muscle; H, heart; S, spinal cord; dc, dorsocervical brown fat depot; iBAT, interscapular brown fat depot. C: Single voxel $^1$H-spectrum from selected region within iBAT (see inset) with eight peaks. The integral value of the $(CH_2)_n$ peak at 1.3 ppm was used as indicator for the lipid content. (A), (B), and (C) were acquired from the same individual. D: $^{31}$P-spectrum from the neck area with the five major peaks. $P_i$, inorganic phosphates; A, adalat capsule marks the center of the surface coil.

9.0 mm$^3$ volume of the neck, including the interscapular and dorsocervical BAT depot, using advanced shimming options of the device. We acquired four spectra of each individual mouse, one before subcutaneous NA injection and three consecutive spectra with an overall time span of 23 min (after injection).

All MRI data were post processed and analyzed with the Syngo software (Siemens Healthcare, Erlangen, Germany).

### Analysis of iBAT volume and composition

The volume of the iBAT (cm$^3$) was calculated for each mouse individually on the basis of sagittal T1-weighted images. The interscapular depot is the biggest of several BAT depots in mice and appears in sagittal slices as a triangular structure in the shoulder region (Fig. 1A, B). To determine the volume of the iBAT, the area of the fat depot was manually drawn on each slice. The sum of all areas was calculated and multiplied by slice thickness (0.08 cm).

The lipid content of BAT was calculated from $^1$H-spectroscopy. Spectroscopic data were post processed as follows: Gaussian-filter with 256 ms width, zero filling to 2,048 points, Fourier transformation, phasing, frequency shift [$(CH_2)_n$ signal was set to 1.3 ppm], baseline correction, frequency shift [$(CH_2)_n$ signal set to 1.3 ppm], curve fitting. This protocol was adapted for the $^1$H-spectrum of each mouse before NA injection and was then used with little adjustments in baseline correction, second frequency shift, and curve fitting for the spectra acquired after injection. The n-methylene peak $(CH_2)_n$ at 1.3 ppm integral value was used as an indicator of lipid content (Fig. 1C). Further, the integral values of the $CH_3$ peak at 0.9 ppm and of the CH=CH peak at 5.3 ppm were determined. The $(CH_2)_n$/CH=CH peak ratio and the CH=CH/$(2/3CH_3)$ peak ratio that represents the mean unsaturation of lipids [according to (35)] were calculated from each spectrum before and 16.5 min after NA injection to get more information about unsaturated fatty acids during thermogenesis. Representative in vivo spectra of white fat have been shown previously (36, 37).

### In vivo measurement of lipid content

In order to calculate the absolute lipid content in milligrams from the $(CH_2)_n$ peak integral value of the $^1$H-spectra, we calibrated our assay with suspensions of oil and water using the same protocol as described for the in vivo measurements. The oil

phantoms (extra virgin olive oil, Brändle, Empfingen, Germany) contained 20, 40, 60, and 80% oil by volume. The mixture was homogenized by ultrasonic disruption (Sonifier B-12, Branson Sonic Power Company, Danbury, CT). The correlation between the known percentage of lipid in the suspension and the $(CH_2)_n$ peak from proton spectroscopy was evaluated and, as a result, a conversion factor of 0.000286 was received that could be used to convert the peak integral values into milligrams of lipid.

### In vivo measurement of energy-rich phosphate levels by phosphorus spectroscopy

Spectroscopic data were post processed with the following protocol: Gaussian-filter with 50 ms width, zero filling to 1,024 points, Fourier transformation, frequency shift [phosphocreatine (PCr) signal was set to 0 ppm], phase correction, baseline correction, frequency shift (PCr signal set to 0 ppm), curve fitting. The post processing protocol was adapted for the $^{31}$P-spectrum of each mouse before NA injection and was then applied to the spectra acquired after injection.

Peak integrals were measured for inorganic phosphate, PCr, and α-, β-, and γ-ATP (Fig. 1D). For the purpose of detecting changes in ATP levels, we nominated the PCr/β-ATP ratio as an indicator for the PCr/ATP ratio and the β-ATP/α-ATP ratio as an indicator for ATP/ADP ratio.

### BAT wet weight

Fourteen mice acclimated at 5°C ambient temperature (six WT mice and eight UCP1-KO mice) were euthanized after the magnetic resonance measurement. The iBAT depot was dissected and immediately weighed (Kern PB, Kern and Sohn GmbH, Germany). A correlation was calculated between iBAT wet weight and the volume of iBAT as estimated via MRI.

### Measurement of oxygen consumption

The metabolic response to NA of mice acclimated to 30°C, 18°C, and 5°C was measured using an open circuit respirometry system with a short response time. Oxygen consumption and carbon dioxide production were measured as it has been described previously (38). Single mice were transferred to 1.8 l cages without food and water and were then placed in a temperature controlled climate chamber at 26°C (KPK 600, Feutron, Germany). A temperature of 26°C, which is just below thermoneutrality, was

chosen to prevent the development of hyperthermia in response to NA injections. Mice were habituated to the calorimetric system for 60–210 min and their resting oxygen consumption was measured. Then the mice were briefly removed from the system for subcutaneous injection of 1 mg NA per kilogram body weight. Air was pumped through the cages with a flow rate of 35 ± 0.5 l/h, dried by an electric freeze trap (M and C Cooler, ECM, Ratingen, Germany) and the airflow was continuously monitored for each channel by an electronic mass flow meter (FM 360, Tylan, München, Germany). $O_2$ and $CO_2$ content of the air were measured with a two-channel $O_2$ analyzer (S3AII, Ametek, Sunnyvale, CA) and a two-channel $CO_2$ analyzer (UNOR 6N, Maihak AG, Hamburg, Germany) with a resolution of 0.001 Δvol% comparing the air entering and leaving the metabolic cuvettes. The readout interval was set to 20 s and the air of an empty cage was measured before and after the NA test and was used for zero readjustment afterwards. The resting metabolic rate of mice was calculated from the lowest mean of 12 consecutive $O_2$ readings, i.e., a 4 min interval. Resting metabolic rate was subtracted from the oxygen consumption after NA injection to acquire the nonshivering thermogenic capacity. This is a standard procedure for the measurement of NST capacity in nonanesthetized mammals and we used it to facilitate comparison of UCP1-KO mice and WT mice as well as comparison with previous studies.

### Statistical analysis

Mean values ± standard error of mean (SEM) are presented. For comparison between the two genotypes a Student's *t*-test for each acclimation temperature was used. When normal distribution of data could not be assumed, the groups were compared with the Mann-Whitney rank sum test. Changes in lipid content and phosphometabolites after NA injection were analyzed by two-way repeated-measures ANOVA followed by a Holm-Sidak comparison test (factors genotype and time point). The acclimation groups (30°C, 18°C, and 5°C) included independent as well as connected measurements where the same mice were measured following acclimation to different temperatures. Therefore, we used the data of each temperature acclimation step for descriptive statistics but analyzed only connected measurements with paired *t*-test statistics. All calculations were performed using SigmaStat 3.5. The overall level of significance was set to $P \leq 0.05$.

### RESULTS

### Heterogeneity of BAT

The iBAT changed its structure during cold acclimation (**Fig. 2**). T1-weighted images revealed that the relatively hyperintense areas of iBAT in warm-acclimated mice, indicating a shorter T1-time due to a higher lipid content, were replaced by hypointense areas, indicating a longer T1-time due to greater water and mitochondria content in cold-acclimated mice (Fig. 2A, B). Using proton spectroscopy, we found a significantly higher lipid content in iBAT of warm-acclimated mice. The lipid content of 30°C-acclimated mice was about three times higher than during cold acclimation at 5°C (**Table 1**). At all acclimation temperatures WT and UCP1-KO mice had the same lipid content in the tissue section used for lipid spectroscopy, i.e., in the core area of iBAT (Fig. 2C). Angiography of the neck area revealed a high vascularization and displayed the arterial vessels of the bilateral interscapular lobes and the Sulzer's vein (supplementary Video I).

Heterogeneity within iBAT was pronounced in WT mice (Fig. 2A) and in UCP1-KO mice (Fig. 2B) acclimated at 18°C. The medial core of iBAT contained more cytoplasm and mitochondria, as indicated by the hypointense signal, whereas the dorsal periphery showed a hyperintense signal. The medial core volume of iBAT was not different in WT compared with UCP1-KO mice at 18°C and 30°C. But it was larger in 5°C-acclimated WT mice than in KO mice ($P = 0.002$). The volume of the whole iBAT did not differ between the genotypes (Fig. 2D).

The iBAT volumes of mice acclimated to 5°C obtained from MRI were compared with their iBAT wet weights. The data indicated a linear relation: y = 1.07 (± 0.4) x + 17.0 (± 40.6) (supplementary Fig. II).

### Lipid loss during NA-induced thermogenesis

We monitored the lipid content of iBAT during NA-induced thermogenesis with consecutive proton spectroscopy. The lipid content in iBAT decreased after NA application in WT mice and in UCP1-KO mice at all acclimation temperatures (**Fig. 3**). This response was faster in WT than in UCP1-KO mice, i.e., the lipid content in WT mice was lowered significantly within 5.5 min after NA injection, while a significant loss of lipids in UCP1-KO mice could first be detected after 11 min. Because cold-acclimated WT and KO mice had lower initial lipid contents, their relative loss of lipids was more pronounced than in warm-acclimated mice (Fig. 3A). The absolute amount of lipid loss was greater in WT mice than in UCP1-KO mice, but it was not affected by the acclimation status of mice (Fig. 3B). It ranged between 9 and 12 mg in WT mice and between 5 and 8 mg in UCP1-KO mice 16.5 min after NA injection (Table 1).

In order to investigate whether fatty acid composition changed during NST we calculated the mean unsaturation ($CH=CH/(2/3CH_3)$) and the $(CH_2)_n/CH=CH$ ratio of iBAT. The ratios did not differ between the genotypes. Mean unsaturation (30°C: WT = 1.3 ± 0.2, KO = 1.9 ± 0.2; 5°C: WT = 3.2 ± 0.6, KO = 2.5 ± 0.2) and the $(CH_2)_n/CH=CH$ ratio (30°C: WT = 11.6 ± 1.6, KO = 9.4 ± 0.7; 5°C: WT = 10.4 ± 0.7, KO = 9.6 ± 0.8) of iBAT were maintained during the first 16.5 min of NA-induced NST.

### Thermogenic response to NA

The injection of NA caused a rapid increase of metabolic rate in WT and UCP1-KO mice, reaching a maximum at about 17 min (**Fig. 4A**). Cold acclimation enhanced the maximal metabolic rate after NA stimulation in WT mice as well as in UCP1-KO mice (Fig. 4B). The increase in maximal thermogenic response following cold acclimation was accompanied by an increase of resting metabolic rate, which was not significantly different between genotypes (Fig. 4C). But the NA-induced capacity for NST (difference between maximum metabolic rate after NA and resting metabolic rate) was about 4-fold greater in cold-acclimated than in warm-acclimated WT mice. UCP1-KO mice also showed an increase of nonshivering thermogenic capacity following cold acclimation (**Table 2**).

The nature of this response to NA was further analyzed by simultaneous recordings of metabolic rate, heart
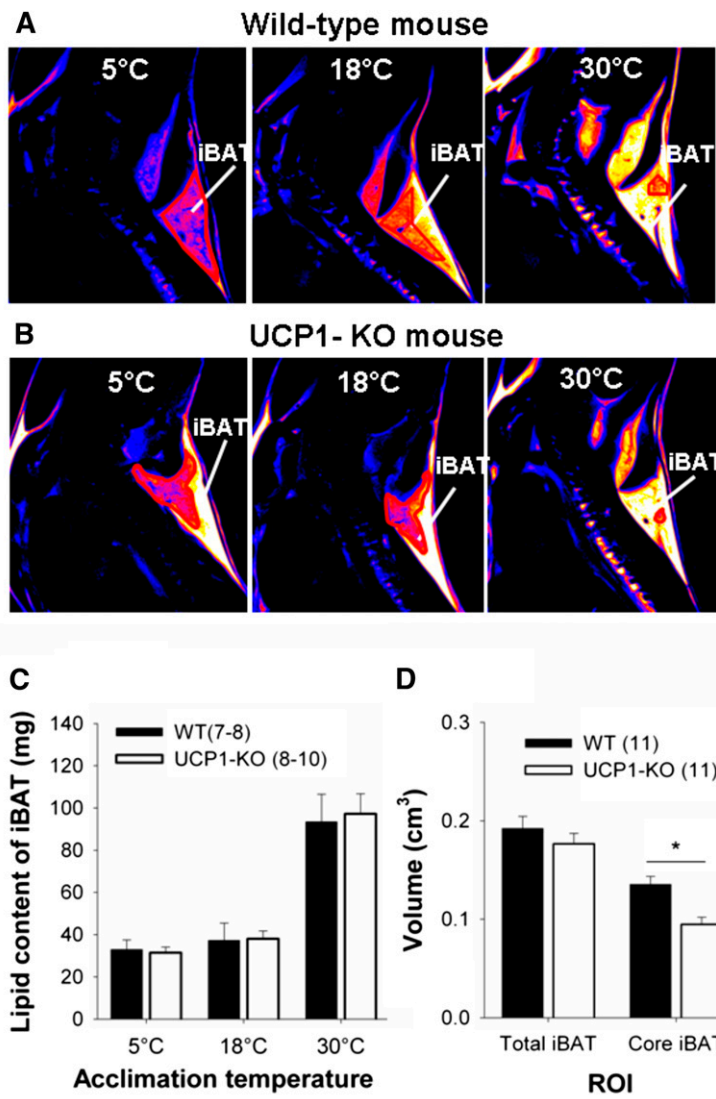
**Fig. 2.** Differences in BAT signal and volume of WT and UCP1- KO mice depending on acclimation temperature and genotype. Representative T1-weighted MR images acquired from a WT mouse (A) and a UCP1-KO mouse (B) sequentially acclimated to 30°C, 18°C, and 5°C. The biggest brown fat depot in the neck area is the iBAT. Images are shown in sagittal view and presented in pseudocolor "hot metal" where bright color encodes for hyperintense signal. C: Lipid content in iBAT of WT and UCP1-KO mice sequentially acclimated to 30°C, 18°C, and 5°C. The $(CH_2)_n$ peak of the proton-spectroscopy was used to calculate the lipid content. D: iBAT volume of WT and UCP1-KO mice acclimated to 5°C. The volume of the total iBAT depot as well as the volume of the darker core region of the iBAT depot [see red line in (A, B)] were calculated. Therefore, the respective areas from each slice were summed up and multiplied by the slice thickness. The core area of the iBAT of WT mice was significantly bigger compared with UCP1-KO mice ($P$ = 0.002).

rate, ventilation rate, and the respiratory quotient in anesthetized mice (supplementary Fig. III). UCP1-KO mice responded to NA by a rapid increase in heart rate, which was identical to the response in WT mice. They also raised their metabolic rate and ventilation rate and showed a slight decrease of the respiratory quotient. These responses were less pronounced than in WT mice.

TABLE 1. Lipid content and lipid loss of BAT during 16.5 min NA-induced thermogenesis

| Acclimation Temperature | Genotype | n | Lipid Content of iBAT before NA (mg)[a] | Lipid Content of iBAT 16.5 min after NA (mg)[a] | Lipid Loss of iBAT (mg/16.5 min) | Estimated Lipid Loss of Total BAT (mg/16.5 min)[b] |
|---|---|---|---|---|---|---|
| 30°C | WT | 8 | 97.19 ± 13.0 | 82.04 ± 11.8 | 11.37 ± 2.5 | 28.42 ± 6.3 |
| | UCP1-KO | 8 | 93.41 ± 9.6 | 88.92 ± 8.7 | 8.28 ± 2.3 | 20.69 ± 5.8 |
| 18°C | WT | 7 | 37.18 ± 8.3 | 25.46 ± 6.0 | 11.72 ± 3.1 | 29.29 ± 7.8 |
| | UCP1-KO | 10 | 38.02 ± 3.8 | 32.28 ± 2.4 | 5.74 ± 1.9 | 14.35 ± 4.7 |
| 5°C | WT | 8 | 32.89 ± 4.6 | 23.63 ± 3.4 | 9.26 ± 1.6 | 23.15 ± 4.1 |
| | UCP1-KO | 10 | 31.37 ± 2.8 | 26.02 ± 2.2 | 5.35 ± 1.8* | 13.38 ± 4.37* |

Calculations are based on proton spectroscopy of the iBAT depot. UCP1-KO and WT mice were sequentially acclimated to ambient temperatures of 30°C, 18°C, and 5°C. Values are means ± SEM. Statistically significant differences between the genotypes at each acclimation temperature ($P \leq 0.05$) are indicated with *.

[a]Calculation of lipid content from proton spectroscopy: lipid (mg) = I × V × A/B. I, integral of $(CH_2)_n$ peak from lipid spectrum; V, iBAT volume regarding MRI; A = 0.000286, conversion factor calculated from oil phantoms with lipid spectroscopy; B = 0.0031 ml, volume of interest in single voxel proton-spectroscopy.

[b]Lipid consumption of total BAT = (lipid content of iBAT before NA − lipid content of iBAT after NA) × 100/40. We estimated that the iBAT accounts for 40% of total BAT. According to Heldmaier (7) iBAT of albino mice makes up 50% of total BAT (without the perirenal depot). According to Thurlby and Trayhurn (21) iBAT of "Aston" mice makes up 34% of total BAT (without periaortic sites). According to own observations iBAT of C57/Bl6 mice represents 52% of total BAT (without perirenal and subventral depots).
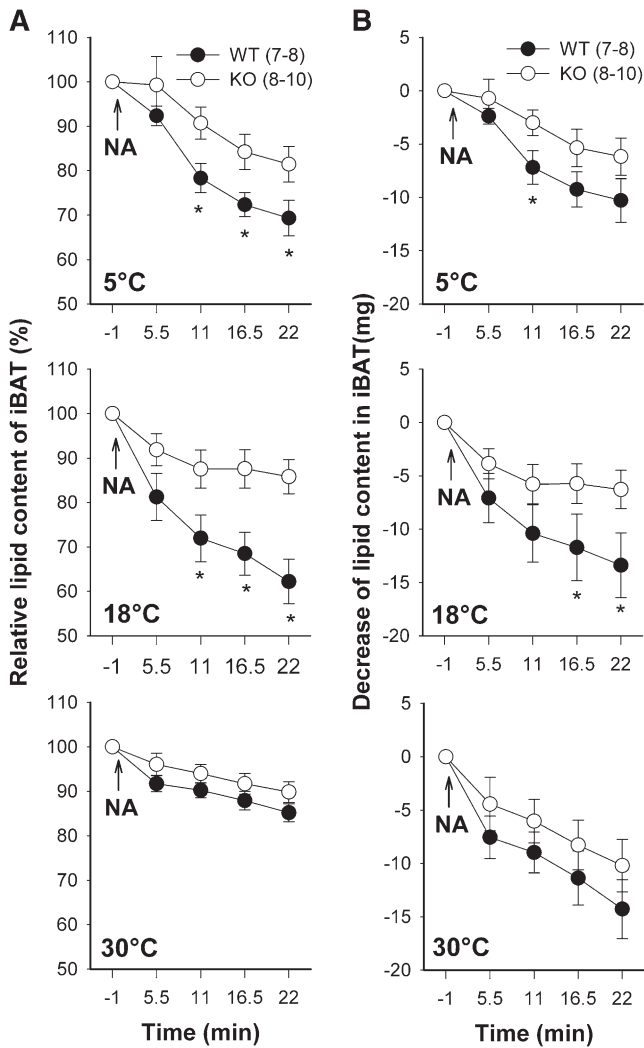
**Fig. 3.** Reduction of lipid content in the iBAT depot of WT and UCP1-KO mice during NA-stimulated NST. Mice were sequentially acclimated to 30°C, 18°C, and 5°C ambient temperature. NA was administered at time point zero and lipid content was monitored over a time span of 22 min after NA injection with consecutive proton spectroscopy using the $(CH_2)_n$ peak as indicator. Lipid content before administration of NA was set to 100% (A). Integral values of the $(CH_2)_n$ peak were converted into milligrams of lipid (B). A statistically significant difference between the genotypes at the same time point ($P \leq 0.05$) is indicated with *. Values are means ± SEM

### In vivo lipid oxidation during NA-induced thermogenesis

Thermogenesis in BAT is fueled by lipids. We evaluated whether the loss of lipid from iBAT was in accordance with the amount of lipid actually oxidized during thermogenesis. The increase of oxygen consumption during 16.5 min of NA-induced thermogenesis was used to calculate the amount of lipids oxidized during this period for each individual mouse (2.01 ml $O_2$ per milligram lipid) (Fig. 4D). WT mice required more lipids to fuel NST than UCP1-KO mice at all acclimation temperatures, as can be expected from the greater metabolic response of WT mice (Fig. 4E, **Table 3**).

However, if these values were compared with the actual depletion of lipids in BAT measured with [1]H-spectroscopy,

it revealed that all mice lost more lipids from BAT than actually required for the thermogenic activity of this tissue (**Fig. 5**). BAT thermogenesis of 5°C-acclimated WT mice, for example, combusted 7.37 mg of lipids during the measurement period of 16.5 min (Table 3), but they actually lost 23.15 mg from BAT during this time (Table 1). In warm-acclimated mice this discrepancy was even greater, they combusted 2.55 mg but lost 28.42 mg of lipids. This discrepancy was also observed in UCP1-KO mice, indicating that lipid loss is not functionally linked to uncoupled respiration of BAT mitochondria. The lipid loss of total BAT was reduced in 5°C-acclimated UCP1-KO as compared with WT mice ($P = 0.046$).

### In vivo ATP levels in BAT during NA-induced thermogenesis

UCP1 uncouples oxidative phosphorylation from the respiratory chain, suggesting that ATP levels in brown adipocytes are changing during NST. Therefore, we analyzed the levels of energy-rich phosphates in BAT in vivo during NA-induced thermogenesis with phosphorus MRS. During thermogenesis the levels of all phosphates were maintained constant. Neither the PCr/ATP ratio (**Fig. 6A**) nor the ATP/ADP ratio (Fig. 6B) showed any response. The phosphate ratios of UCP1-KO mice, which cannot uncouple ATP synthesis from the respiratory chain, were identical with the phosphate ratios measured in WT mice. We pooled the data of WT and UCP1-KO mice before NA injection and found a significantly lower ($P = 0.035$) PCr/ATP ratio in cold-acclimated mice (3.16 ± 0.27) than following 30°C acclimation (4.02 ± 0.27). The ATP/ADP ratio showed a trend ($P = 0.062$) to higher values in cold-acclimated mice. Both results indicated an increased ATP level in the iBAT of cold-acclimated mice.

## DISCUSSION

### Structural changes of BAT during cold acclimation

The iBAT depot of mice did not present a uniform structure in our T1-weighted images, but it separated into a hypointense core and a relatively hyperintense dorsal periphery. This suggests a core area where brown adipocytes contain more cytoplasm and mitochondria, and thus the potential for a greater metabolic activity. In contrast, the brown adipocytes in the peripheral area are rich in lipids and contain less cytoplasm and mitochondria. An internal differentiation of BAT was not visible with CT imaging (39), while different layers of interscapular brown fat were described before in rats and mice using MRI (30, 32). Activation of BAT with adrenaline confirmed a higher metabolic activity in the core region of this organ (40). In mice, metabolically active BAT has been detected recently with T2-weighted MRI, as a signal loss of about 20% occurred due to decreased blood oxygenation in the tissue (41).

During cold adaptation, the hypointense core area of the interscapular lobe expanded toward the periphery. In 5°C-acclimated WT mice the entire interscapular lobe
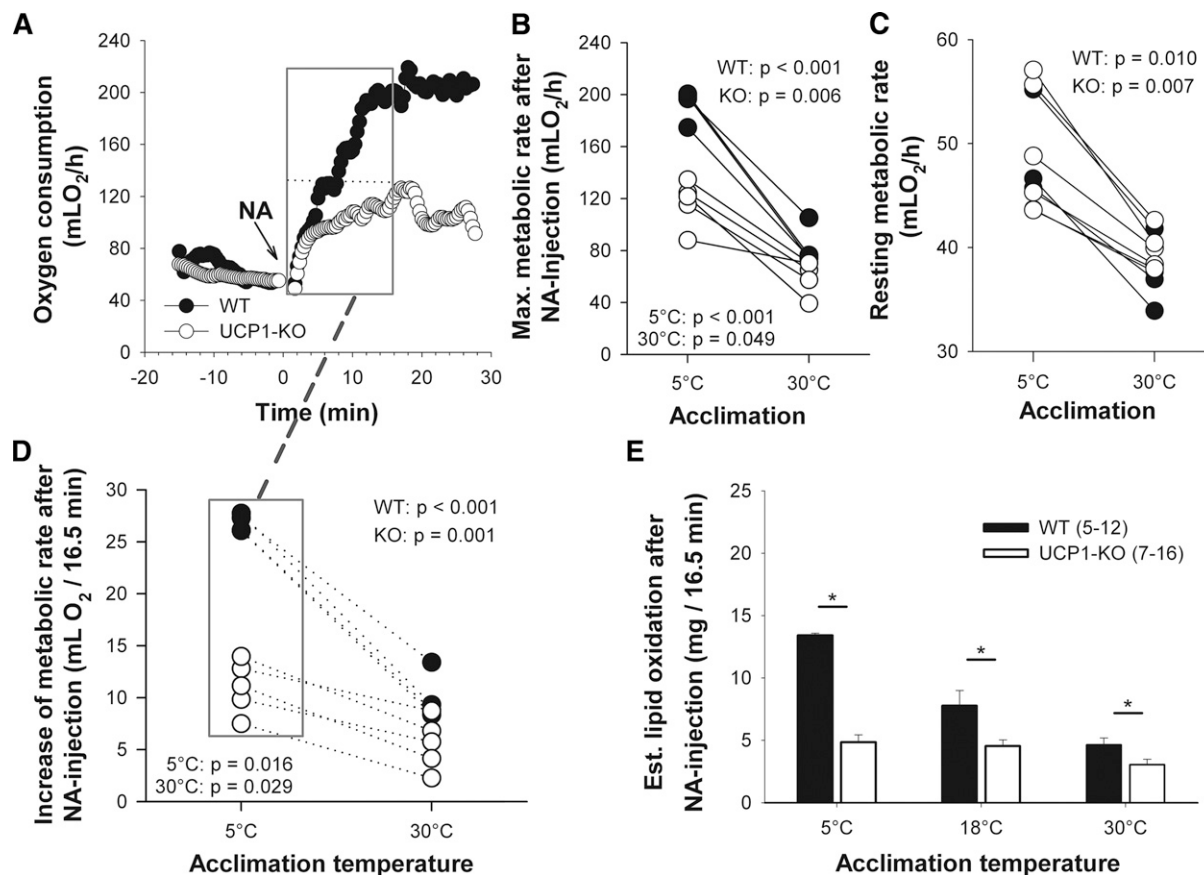
**Fig. 4.** Metabolic responses of mice to NA measured by indirect calorimetry. Representative oxygen consumption of a WT and a UCP1-KO mouse acclimated to 5°C ambient temperature (A). NA was injected at time point zero. Maximum (Max.) metabolic rate reached after NA injection (B) and resting metabolic rate (C) of the same individuals (WT mice, n = 4; UCP1-KO mice, n = 5) following 30°C and 5°C acclimation. The number of animals is lower than in Tables 2 and 3 because only connected measurements were included in the graph (corresponding values are connected by lines). The increase of metabolic rate during 16.5 min of NA-induced thermogenesis (D) (see gray box in A) was used to calculate the amount of oxidized lipids during this time span (E). For calculation of lipid oxidation, it was assumed that solely palmitate was metabolized. Values are means ± SEM. A statistically significant difference between the genotypes at each acclimation temperature ($P \leq 0.05$) is indicated with *.

became hypointense, i.e., all adipocytes were converted into the metabolically active form with a reduced lipid content, indicating a higher metabolic and thermogenic capacity. Cold-acclimated UCP1-KO mice also showed a core area with reduced lipid content in their iBAT, but only a part of the tissue lobe converted into the metabolically active form. Cold adaptive changes of BAT largely depend upon the activity of its sympathetic innervation

(42, 43), as has been demonstrated in studies about denervation of BAT (44–47). The present findings show that the reorganization of BAT during cold acclimation toward an improvement of its thermogenic capacity occurs in the absence of UCP1, although a slightly reduced intensity was observed as compared with WT mice. This suggests a feedback of UCP1 or uncoupled mitochondrial respiration on the full deployment of BAT thermogenic capacity.

TABLE 2. Resting metabolic rate, maximal metabolic rate after NA, and capacity of NST

| Acclimation Temperature | Genotype | n | Resting Metabolic Rate[a] | Maximal Metabolic Rate after NA[a] | NST Capacity after NA[a] |
|---|---|---|---|---|---|
| 30°C | WT | 5 | 36.65 ± 1.6 | 75.97 ± 8.9 | 39.32 ± 7.5 |
| | UCP1-KO | 7 | 41.17 ± 1.3 | 61.07 ± 4.7 | 19.90 ± 4.2* |
| 18°C | WT | 12 | 46.23 ± 0.9 | 175.21 ± 3.6 | 128.98 ± 3.8 |
| | UCP1-KO | 16 | 46.01 ± 0.9 | 96.48 ± 2.9* | 50.47 ± 2.8* |
| 5°C | WT | 5 | 47.21 ± 2.1 | 200.77 ± 9.4 | 153.56 ± 10.1 |
| | UCP1-KO | 7 | 47.52 ± 2.5 | 107.46 ± 8.3* | 59.94 ± 7.0* |

NST capacity is the difference between resting metabolic rate and maximum metabolic rate after NA injection. UCP1-KO and WT mice were sequentially acclimated to ambient temperatures of 30°C, 18°C, and 5°C. Values are means ± SEM. Statistically significant differences between the genotypes at each acclimation temperature ($P \leq 0.05$) are indicated with *.
[a]Values are in milliliters of $O_2$ per hour.

TABLE 3.   Increase of metabolic rate and the estimated lipid oxidation of mice during 16.5 min NA-induced thermogenesis

| Acclimation Temperature | Genotype | n | Increase of Metabolic Rate[a,b] | Estimated Lipid Oxidation of Whole Body[a,c] | Estimated Lipid Oxidation of Total BAT[a,d] |
|---|---|---|---|---|---|
| 30°C | WT | 5 | 9.31 ± 1.1 | 4.63 ± 0.6 | 2.55 ± 0.3 |
|  | UCP1-KO | 7 | 6.12 ± 0.9* | 3.04 ± 0.4* | 1.67 ± 0.2* |
| 18°C | WT | 12 | 23.34 ± 0.9 | 11.60 ± 0.5 | 6.38 ± 0.3 |
|  | UCP1-KO | 16 | 10.30 ± 0.6* | 5.12 ± 0.3* | 2.82 ± 0.15* |
| 5°C | WT | 5 | 26.98 ± 0.4 | 13.41 ± 0.2 | 7.37 ± 0.1 |
|  | UCP1-KO | 7 | 9.76 ± 1.2* | 4.85 ± 0.6* | 2.67 ± 0.3* |

Lipid oxidation is calculated from original measurements of oxygen consumption measured via indirect calorimetry. UCP1-KO and WT mice were sequentially acclimated to ambient temperatures of 30°C, 18°C, and 5°C. Values are means ± SEM. Statistically significant differences between the genotypes at each acclimation temperature ($P \leq 0.05$) are indicated with *.
  [a]Values are in milliliters of $O_2$ per 16.5 min.
  [b]Increase of metabolic rate (milliliters of $O_2$/16.5 min) = amount of consumed oxygen after NA injection in 16.5 min − resting metabolic rate.
  [c]Lipid oxidation whole body = metabolic rate (milliliters of $O_2$)/A × B. A = 515.2 l $O_2$/mol palmitate, necessary amount of oxygen for oxidation of 1 mol palmitate; B = 256 g/mol, molar weight of palmitate.
  [d]Lipid oxidation of total BAT = lipid oxidation whole body × 0.55, estimating that BAT contributes 55% of NST [Thurlby and Trayhurn (21)].

## BAT ATP levels during thermogenesis

BAT mitochondria have a relatively low capacity for ATP synthesis as compared with their respiratory potential [for review see (48)]. During thermogenesis mitochondrial respiration is uncoupled from ATP synthesis, including the risk that ATP levels in the cells are coming under pressure. Therefore, we analyzed the phosphate levels during NA-induced thermogenesis in vivo by MRS. Cold-acclimated mice had slightly lower PCr/ATP ratios and slightly higher ATP/ADP ratios, but these ratios did not change during sympathetic activation of thermogenesis, neither in WT nor in UCP1-KO mice. The constant ATP/ADP ratio suggests that ATP is still generated at a sufficient rate to cover the cellular needs for enzyme activation and biosynthesis. Maintenance of ATP levels during thermogenesis should be especially demanding for WT mice, whereas UCP1-KO mice should face no problems with ATP supply. The stable ATP levels in WT mice indicate that either oxidative phosphorylation is not completely prevented during NST or that other sources of ATP may compensate for mitochondrial deficits of ATP production, e.g., glycolysis (49). BAT utilizes glucose at high rates and may consume up to 12.5% of the entire glucose consumption in mice, although it amounts to only about 1% of total body mass (50). Glucose may be used for synthesis of fatty acids as well as for a glycolytic breakdown to pyruvate, lactate, and acetyl-CoA. During thermogenic stimulation rats released lactate and pyruvate from BAT accounting for 33% of the glucose uptake (51). This suggests an enhancement of glycolysis which could be a potential source of ATP. Cold acclimation also increases the activity of key enzymes for glycolysis, indicating that an increase in the capacity for uncoupled respiration is accompanied by an enhancement of glycolysis (52).

## BAT lipid metabolism during thermogenesis

During NA-induced NST the lipid content of BAT decreased by about 30% within 16.5 min. A loss of lipids can be expected because β-adrenergic thermogenesis in BAT is largely fueled by lipids [for review see (3)]. However, the absolute amount of lipids decreased from BAT was much greater than could have been consumed during thermogenesis, e.g., cold-acclimated WT mice lost three times the amount of lipids that were required for thermogenesis in brown fat, as calculated from oxygen consumption during the same period of time. In warm-acclimated mice this discrepancy was even greater, i.e., 11 times more lipids were lost from BAT than actually consumed. For the direct comparison of lipid loss acquired from MRS and lipid oxidation acquired from indirect calorimetry, we assumed that iBAT represents 40% of total BAT (see footnotes of Table 1). So, the projected results of lipid loss and lipid oxidation are estimates. However, these are minimum estimates because lipid loss was measured in anesthetized mice during 16.5 min with MRS, whereas the metabolic rate for NST was measured for 16.5 min in nonanesthetized mice. Anesthesia reduces resting metabolic rate prior to NA as well as the maximal metabolic response to NA. The combination of both effects may reduce peak metabolic rates by up to 50% (11, 53) suggesting that lipid turnover is also reduced during MRS in anesthetized mice as compared with nonanesthetized mice. Considering the fact that NA-induced thermogenesis also increases glucose uptake and utilization in BAT, we suggest that the lipid oxidation is lower as assumed and lipid loss may be even greater than 11 times as compared with metabolic rate (51, 54).

An exaggerated mobilization and export of fatty acids from adipocytes was also observed in vitro following noradrenergic stimulation (18, 55, 56). The in vitro observations suggest that the export of fatty acids is a native property of brown adipocyte metabolism. In vivo studies measuring plasma levels and arteriovenous concentration differences revealed a release of glycerol and fatty acids from BAT during cold exposure, as well as β-adrenergic stimulation in mice (57, 58), rats (51, 59), and in humans (60). In Djungarian hamsters the plasma level of fatty acids was almost doubled during NA-induced thermogenesis,
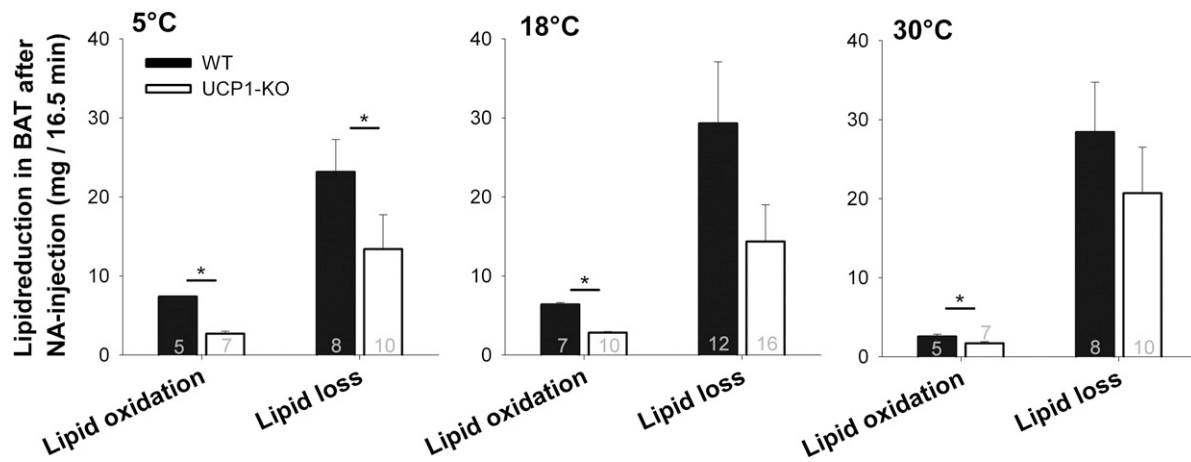
**Fig. 5.** Change in lipid levels through lipid oxidation and lipid loss in total BAT during 16.5 min NA-induced thermogenesis. WT and UCP1-KO mice were sequentially acclimated to 30°C, 18°C, and 5°C. Lipid loss and lipid oxidation were calculated over a time period of 16.5 min. Sample sizes are shown inside bars. Values are means ± SEM. Statistically significant differences in lipid loss or lipid oxidation comparing WT and UCP1-KO mice at each acclimation temperature ($P \leq 0.05$) are indicated with *.

as well as during cold exposure, and the release of fatty acids could be inhibited by blockade of adrenergic β-receptors (19).

Cold exposure and β-adrenergic stimulation of thermogenesis not only mobilize fatty acids in BAT, but also stimulate the uptake of fatty acids as was demonstrated in mice and humans (60, 61). Lipoprotein lipase is anchored to the periphery of brown adipocytes and liberates fatty acids from circulating lipoproteins, thus allowing the import of fatty acids. The activity of this enzyme is rapidly increased during cold exposure (13, 62, 63). This demonstrates that β-adrenergic stimulation of BAT simultaneously increases lipolysis and the oxidation of fatty acids as well as the uptake and the export of fatty acids, i.e., the turnover of lipids is exaggerated well beyond its need for fueling BAT metabolism. This response of BAT supports the view that its sympathetic activation induces heat production via UCP1 and additionally enhances triglyceride clearance (61). The mechanism of fatty acid action on UCP1 activation and on proton conductance of the mitochondrial membrane is still not clear. Current hypotheses prefer a direct action on UCP1 and suggest a flip-flop model or that fatty acids act as a cofactor on UCP1 (64, 65). No matter which mechanism might be in operation, the high turnover of lipids and fatty acids provides a high intracellular level of long chain fatty acids, thus facilitating the thermogenic uncoupling of brown fat mitochondria.

### Physiological role of brown fat

BAT is considered to be the main contributor to NST in small mammals, but the magnitude of its contribution and the involvement of other tissues are still unclear. Blood flow studies with radioactively labeled microspheres estimate that about 60% of the thermogenic response is due to brown fat metabolic activity in rats, mice, and hamsters (21, 66, 20). In turn this indicates that other tissues contribute to total NST. Surgical removal of BAT or tying the Sulzer vein caused rather complex results. In one report rats did not reduce their capacity for NST immediately

following removal of the interscapular lobe of brown fat (67), whereas other studies reported a reduction of the thermogenic capacity by about 16% (68, 69). In a more detailed study with stepwise partial removal of BAT from several lobes in Djungarian hamsters, it was estimated that in warm-acclimated hamsters 50% of NST can be ascribed to the respiratory capacity of BAT and this percentage increases to 85% following cold adaptation (70), indicating that 50% and 15% of heat is generated by other tissues, respectively.
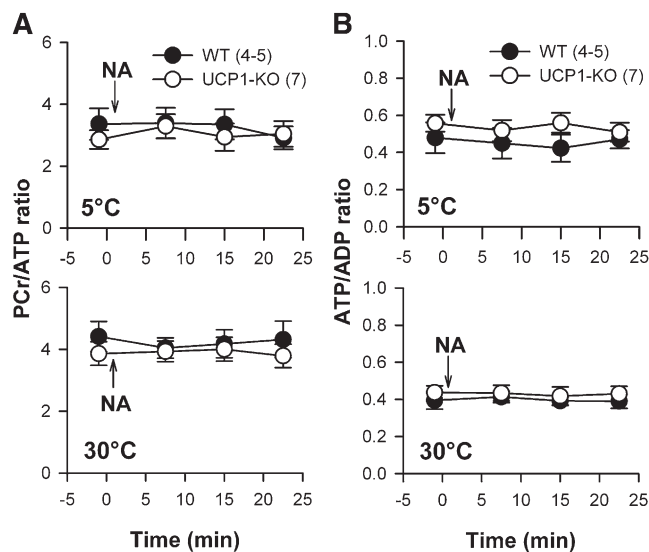


**Fig. 6.** PCr/ATP ratio (A) and ATP/ADP ratio (B) during NA-induced thermogenesis in WT and UCP1-KO mice acclimated to 30°C and 5°C ambient temperature. ^{31}P-spectroscopy was performed before and three times after NA stimulation in the neck region of mice. The β-ATP peak from the phosphate spectrum represents mainly ATP and was therefore used as ATP index. The α-ATP peak contains signal from ATP and ADP molecules. Therefore, the β-ATP/α-ATP peak ratio reflects the ATP/ADP ratio. Values are means ± SEM.

UCP1-KO mice can tolerate long term exposure to 4°C after a stepwise reduction of ambient temperature (23, 26, 71). In the present study, we showed a thermogenic response to NA which was enhanced following cold acclimation, indicating an adaptive increase of NST despite the lack of UCP1 in brown adipocytes. In accordance with our results, a thermogenic response to NA in UCP1-KO and UCP1-dta mice has been described previously (23, 72). In contrast, Golozoubova et al. (24), Nedergaard et al. (71), and Cannon and Nedergaard (73) did not observe an increase in the noradrenergic thermogenic response in these mice following cold acclimation at 18°C and therefore define "adaptive NST" as strictly limited to UCP1-mediated uncoupling of oxidative phosphorylation in brown adipocytes. They explain the increased cold tolerance of UCP1-KO mice by an adaptive improvement of shivering thermogenesis (24, 71, 73). However, cold-adapted UCP1-KO mice did not show any changes in gene expression, mitochondrial DNA, or respiratory capacity of isolated muscle tissue, which could support an increased contribution of skeletal muscle tissue to thermogenesis (23, 26, 72). During NA-induced thermogenesis, blood flow in skeletal muscle remained constant or even decreased, which contradicts a significant contribution to NST (20, 21, 66). Blood flow through the ventricular muscle tissue increased during NST and this response was enhanced following cold acclimation (20). In the current study, we observed a prominent increase of heart rate in WT and UCP1-KO mice (supplementary Fig. III), supporting the view that enhanced cardiovascular activity contributes to the UCP1-independent nonshivering thermogenic response.

More and more evidence is accumulating that heat dissipation from BAT is supported by white adipose tissue in order to maintain body temperature. During cold exposure, white adipose tissue of UCP1-KO mice shows changes in gene expression, enzyme activities, and cytochrome c oxidase activity as well as an increase of mRNA levels, suggesting that white adipose tissue may contribute to the adaptive improvement of NST (23, 26). In WT mice, UCP1-expressing beige adipocytes with an enhanced respiratory capacity can be recruited within white adipose tissue depots and may be involved in the global lipid clearance during NST (26, 74–76). Cold acclimation stimulates the recruitment of these cells and this response may be enhanced by a paucity of BAT cells (77).

Thermogenesis itself requires cooperation of brown and white adipose tissue. The noradrenergic stimulation of brown adipocytes causes lipolysis and reesterification simultaneously and a large portion of liberated fatty acids are exported into the bloodstream raising the plasma level of FFAs. The high rate of lipid mobilization in UCP1-KO mice in our study suggests that lipid cycling is not functionally linked to the presence of UCP1. In birds, which entirely lack UCP1, an activation of white adipocytes was observed when mesenchymal stem cells were treated with PPARγ, a coactivator which is specific for the differentiation of brown adipocytes. This indicates that the potential for activation of white adipose tissue is a physiological property separate from the evolutionary presence of UCP1

(78). Recently it has been demonstrated that the respiratory capacity of white adipose tissue, and potentially also of BAT, may be enhanced by the presence of n-3 polyunsaturated fatty acids in the absence of UCP1 (79, 80). This increased turnover of n-3 polyunsaturated fatty acids could not be corroborated in our study, as the saturation index of BAT lipids did not change during NST.

The cycling of lipolysis and reesterification of lipids can also be enhanced by β-adrenergic stimulation in isolated white adipocytes [see (81, 82) for review]. During prolonged cold exposure, BAT requires a continuous supply of fatty acids to fuel thermogenesis and these can only be provided by the much larger depots of white adipose tissue. In summary, this suggests a tight functional link of brown and white adipose tissue thermogenesis and cold acclimation.

The simultaneous activation of lipolysis and reesterification suggests a futile cycling of lipid metabolism (83) and consumes 8 mol of ATP per release and reesterification of three molecules of fatty acids (80). This could even generate heat in white adipose tissue, provided there is a sufficient supply of ATP. The apparently unnecessary large capacity for lipolysis and lipid cycling in BAT suggests that the tissue is also a major effector of triglyceride clearance (61). Neither the excitation of lipid cycling nor the adaptive modification of brown or white adipocytes for mitochondrial proliferation and multilocular lipid storage requires UCP1, as we found in our study in accordance with (26, 80). This suggests that the mechanism of lipid clearance could be considered as a separate physiological function of BAT, in addition to its role in thermogenesis. The recent discovery of brown and beige adipose tissue in humans (76, 84, 85) may further elucidate this view. The amount of BAT in humans in relation to the body mass is quite small, and thus it may generate only small amounts of heat. However, recent evidence indicates that brown adipose mass and activity in humans is highly variable and can change in response to the nutritional state, ambient temperature, photoperiod, etc., and a positive contribution of thermogenically activated brown fat on energy expenditure may have been underestimated in the past [for review see (86)]. Lipid cycling induced in BAT during thermogenesis exceeds the fuel needs for thermogenesis by far. Its potential effect on lipid clearance may dominate over its thermogenic role, thus explaining and promising a beneficial effect of human BAT on the prevention of atherosclerosis, cardiovascular diseases, and obesity (16, 75). ∎

## REFERENCES

1. Hull, D. 1966. The structure and function of brown adipose tissue. *Br. Med. Bull.* **22:** 92–96.
2. Heldmaier, G., H. Böckler, A. Buchberger, G. R. Lynch, W. Puchalski, S. Steinlechner, and H. Wiesinger. 1985. Seasonal acclimation and thermogenesis. *In* Circulation, Respiration, and

Metabolism. R. Gilles, editor. Springer-Verlag, Berlin, Heidelberg. 490–501.

3. Cannon, B., and J. A. N. Nedergaard. 2004. Brown adipose tissue: function and physiological significance. *Physiol. Rev.* **84:** 277–359.

4. Heldmaier, G., S. Steinlechner, J. Rafael, and P. Vsiansky. 1981. Photoperiodic control and effects of melatonin on nonshivering thermogenesis and brown adipose tissue. *Science.* **212:** 917–919.

5. Bukowiecki, L., A. J. Collet, N. Follea, G. Guay, and L. Jahjah. 1982. Brown adipose tissue hyperplasia: a fundamental mechanism of adaptation to cold and hyperphagia. *Am. J. Physiol.* **242:** E353–E359.

6. Golozoubova, V., H. Gullberg, A. Matthias, B. Cannon, B. Vennström, and J. Nedergaard. 2004. Depressed thermogenesis but competent brown adipose tissue recruitment in mice devoid of all hormone-binding thyroid hormone receptors. *Mol. Endocrinol.* **18:** 384–401.

7. Heldmaier, G. 1974. Temperature adaptation and brown adipose tissue in hairless and albino mice. *J. Comp. Physiol.* **92:** 281–292.

8. Ashwell, M., G. Jennings, D. Richard, D. M. Stirling, and P. Trayhurn. 1983. Effect of acclimation temperature on the concentration of the mitochondrial "uncoupling" protein measured by radioimmunoassay in mouse brown adipose tissue. *FEBS Lett.* **161:** 108–112.

9. Lowell, B. B., and B. M. Spiegelman. 2000. Towards a molecular understanding of adaptive thermogenesis. *Nature.* **404:** 652–660.

10. Smith, R. E., and J. C. Roberts. 1964. Thermogenesis of brown adipose tissue in cold-acclimated rats. *Am. J. Physiol.* **206:** 143–148.

11. Heldmaier, G. 1971. Zitterfreie Wärmebildung und Körpergröße bei Säugetieren. *Z. Vgl. Physiol.* **73:** 222–248.

12. Foster, D. O., and M. L. Frydman. 1979. Tissue distribution of cold-induced thermogenesis in conscious warm- or cold-acclimated rats reevaluated from changes in tissue blood flow: the dominant role of brown adipose tissue in the replacement of shivering by nonshivering thermogenesis. *Can. J. Physiol. Pharmacol.* **57:** 257–270.

13. Carneheim, C., J. Nedergaard, and B. Cannon. 1984. Beta-adrenergic stimulation of lipoprotein lipase in rat brown adipose tissue during acclimation to cold. *Am. J. Physiol.* **246:** E327–E333.

14. Portet, R., M. C. Laury, R. Bertin, C. Senault, M. T. Hluszko, L. Chevillard, and J. Le Blanc. 1974. Hormonal stimulation of substrate utilization in brown adipose tissue of cold acclimated rats. *Proc. Soc. Exp. Biol. Med.* **147:** 807–812.

15. LaFrance, L., G. Lagacé, and D. Routhier. 1980. Free fatty acid turnover and oxygen consumption. Effects of noradrenaline in nonfasted and nonanesthetized cold-adapted rats. *Can. J. Physiol. Pharmacol.* **58:** 797–804.

16. Bartelt, A., M. Merkel, and J. Heeren. 2012. A new, powerful player in lipoprotein metabolism: brown adipose tissue. *J. Mol. Med.* **90:** 887–893.

17. Hagberg, C. E., A. Falkevall, X. Wang, E. Larsson, J. Huusko, I. Nilsson, L. A. van Meeteren, E. Samen, L. Lu, M. Vanwildemeersch, et al. 2010. Vascular endothelial growth factor B controls endothelial fatty acid uptake. *Nature.* **464:** 917–921.

18. Nedergaard, J., and O. Lindberg. 1979. Norepinephrine-stimulated fatty-acid release and oxygen consumption in isolated hamster brown- fat cells. Influence of buffers, albumin, insulin and mitochondrial inhibitors. *Eur. J. Biochem.* **95:** 139–145.

19. Heldmaier, G., and K. Seidl. 1985. Plasma free fatty acid levels during cold-induced and noradrenaline-induced nonshivering thermogenesis in the Djungarian hamster. *J. Comp. Physiol. B.* **155:** 679–684.

20. Puchalski, W., H. Böckler, G. Heldmaier, and M. Langefeld. 1987. Organ blood flow and brown adipose tissue oxygen consumption during noradrenaline-induced nonshivering thermogenesis in the Djungarian hamster. *J. Exp. Zool.* **242:** 263–271.

21. Thurlby, P. L., and P. Trayhurn. 1980. Regional blood flow in genetically obese (ob/ob) mice. The importance of brown adipose tissue to the reduced energy expenditure on non-shivering thermogenesis. *Pflugers Arch.* **385:** 193–201.

22. Inokuma, K., Y. Okamatsu-Ogura, A. Omachi, Y. Matsushita, K. Kimura, H. Yamashita, and M. Saito. 2006. Indispensable role of mitochondrial UCP1 for antiobesity effect of beta3-adrenergic stimulation. *Am. J. Physiol. Endocrinol. Metab.* **290:** E1014–E1021.

23. Meyer, C. W., M. Willershäuser, M. Jastroch, B. C. Rourke, T. Fromme, R. Oelkrug, G. Heldmaier, and M. Klingenspor. 2010. Adaptive thermogenesis and thermal conductance in wild-type and UCP1-KO mice. *Am. J. Physiol. Regul. Integr. Comp. Physiol.* **299:** R1396–R1406.

24. Golozoubova, V., E. Hohtola, A. Matthias, A. Jacobsson, B. Cannon, and J. Nedergaard. 2001. Only UCP1 can mediate adaptive nonshivering thermogenesis in the cold. *FASEB J.* **15:** 2048–2050.

25. Granneman, J. G., M. Burnazi, Z. Zhu, and L. A. Schwamb. 2003. White adipose tissue contributes to UCP1-independent thermogenesis. *Am. J. Physiol. Endocrinol. Metab.* **285:** E1230–E1236.

26. Ukropec, J., R. P. Anunciado, Y. Ravussin, M. W. Hulver, and L. P. Kozak. 2006. UCP1-independent thermogenesis in white adipose tissue of cold-acclimated Ucp1-/- mice. *J. Biol. Chem.* **281:** 31894–31908.

27. Hu, H. H., D. L. Smith, K. S. Nayak, M. I. Goran, and T. R. Nagy. 2010. Identification of brown adipose tissue in mice with fat-water IDEAL-MRI. *J. Magn. Reson. Imaging.* **31:** 1195–1202.

28. Peng, X-G., S. Ju, F. Fang, Y. Wang, K. Fang, X. Cui, G. Liu, P. Li, H. Mao, and G-J. Teng. 2013. Comparison of brown and white adipose tissue fat fractions in ob, seipin, and Fsp27 gene knockout mice by chemical shift-selective imaging and (1)H-MR spectroscopy. *Am. J. Physiol. Endocrinol. Metab.* **304:** E160–E167.

29. Holstila, M., K. A. Virtanen, T. J. Grönroos, J. Laine, V. Lepomäki, J. Saunavaara, I. Lisinen, M. Komu, J. C. Hannukainen, P. Nuutila, et al. 2013. Measurement of brown adipose tissue mass using a novel dual-echo magnetic resonance imaging approach: a validation study. *Metabolism.* **62:** 1189–1198.

30. Lunati, E., P. Marzola, E. Nicolato, M. Fedrigo, M. Villa, and A. Sbarbati. 1999. In vivo quantitative lipidic map of brown adipose tissue by chemical shift imaging at 4.7 Tesla. *J. Lipid Res.* **40:** 1395–1400.

31. Hu, H. H., C. D. G. Hines, D. L. Smith, and S. B. Reeder. 2012. Variations in $T(2)^*$ and fat content of murine brown and white adipose tissues by chemical-shift MRI. *Magn. Reson. Imaging.* **30:** 323–329.

32. Smith, D. L., Y. Yang, H. H. Hu, G. Zhai, and T. R. Nagy. 2013. Measurement of interscapular brown adipose tissue of mice in differentially housed temperatures by chemical-shift-encoded water-fat MRI. *J. Magn. Reson. Imaging.* **38:** 1425–1433.

33. Enerbäck, S., A. Jacobsson, E. M. Simpson, C. Guerra, H. Yamashita, M. E. Harper, and L. P. Kozak. 1997. Mice lacking mitochondrial uncoupling protein are cold-sensitive but not obese. *Nature.* **387:** 90–94.

34. Klingenspor, M., C. Ebbinghaus, G. Hiilshorst, S. Stiihr, F. Spiegelhalter, K. Haas, and G. Heldmaier. 1996. Multiple regulatory steps are involved in the control of lipoprotein lipase activity in brown adipose tissue. *J. Lipid Res.* **37:** 1685–1695.

35. Zancanaro, C., R. Nano, C. Marchioro, A. Sbarbati, A. Boicelli, and F. Osculati. 1994. Magnetic resonance spectroscopy investigations of brown adipose tissue and isolated brown adipocytes. *J. Lipid Res.* **35:** 2191–2199.

36. Calderan, L., P. Marzola, E. Nicolato, P. F. Fabene, C. Milanese, P. Bernardi, A. Giordano, S. Cinti, and A. Sbarbati. 2006. In vivo phenotyping of the ob/ob mouse by magnetic resonance imaging and 1H-magnetic resonance spectroscopy. *Obesity (Silver Spring).* **14:** 405–414.

37. Strobel, K., J. van den Hoff, and J. Pietzsch. 2008. Localized proton magnetic resonance spectroscopy of lipids in adipose tissue at high spatial resolution in mice in vivo. *J. Lipid Res.* **49:** 473–480.

38. Heldmaier, G., and T. Ruf. 1992. Body temperature and metabolic rate during natural hypothermia in endotherms. *J. Comp. Physiol. B.* **162:** 696–706.

39. Lubura, M., D. Hesse, N. Neumann, S. Scherneck, P. Wiedmer, and A. Schürmann. 2012. Non-invasive quantification of white and brown adipose tissues and liver fat content by computed tomography in mice. *PLoS ONE.* **7:** e37026.

40. Sbarbati, A., I. Cavallini, P. Marzola, E. Nicolato, and F. Osculati. 2006. Contrast-enhanced MRI of brown adipose tissue after pharmacological stimulation. *Magn. Reson. Med.* **55:** 715–718.

41. Khanna, A., and R. T. Branca. 2012. Detecting brown adipose tissue activity with BOLD MRI in mice. *Magn. Reson. Med.* **68:** 1285–1290.

42. Girardier, L., and J. Seydoux. 1986. Neural control of brown adipose tissue. *In* Brown Adipose Tissue. P. Trayhurn and D. G. Nicholls, editors. Edward Arnold Ltd., London. 122–151.

43. Park, I. R., and J. Himms-Hagen. 1988. Neural influences on trophic changes in brown adipose tissue during cold acclimation. *Am. J. Physiol.* **255:** R874–R881.

44. Foster, D. O., F. Depocas, and G. Zaror-Behrens. 1982. Unilaterality of the sympathetic innervation of each pad of rat interscapular brown adipose tissue. *Can. J. Physiol. Pharmacol.* **60:** 107–113.

45. Hamilton, J. M., T. J. Bartness, and G. N. Wade. 1989. Effects of norepinephrine and denervation on brown adipose tissue in Syrian hamsters. *Am. J. Physiol.* **257:** R396–R404.

46. Meywirth, A., U. Redlin, S. Steinlechner, G. Heldmaier, and R. J. Reiter. 1991. Role of the sympathetic innervation in the cold-induced activation of 5′-deiodinase in brown adipose tissue of the Djungarian hamster. *Can. J. Physiol. Pharmacol.* **69:** 1896–1900.

47. Klingenspor, M., A. Meywirth, S. Stöhr, and G. Heldmaier. 1994. Effect of unilateral surgical denervation of brown adipose tissue on uncoupling protein mRNA level and cytochrome-c-oxidase activity in the Djungarian hamster. *J. Comp. Physiol. B.* **163:** 664–670.

48. Nicholls, D. G., and R. M. Locke. 1984. Thermogenic mechanisms in brown fat. *Physiol. Rev.* **64:** 1–64.

49. Himms-Hagen, J. 1990. Brown adipose tissue thermogenesis: interdisciplinary studies. *FASEB J.* **4:** 2890–2898.

50. Young, P., M. A. Cawthorne, and S. A. Smith. 1985. Brown adipose tissue is a major site of glucose utilisation in C57Bl/6 ob/ob mice treated with a thermogenic beta-adrenoceptor agonist. *Biochem. Biophys. Res. Commun.* **130:** 241–248.

51. Ma, S. W. Y., and D. O. Foster. 1986. Uptake of glucose and release of fatty acids and glycerol by rat brown adipose tissue in vivo. *Can. J. Physiol. Pharmacol.* **64:** 609–614.

52. Heldmaier, G., S. Klaus, H. Wiesinger, U. Friedrichs, and M. Wenzel. 1989. Cold acclimation and thermogenesis. *In* Living in the Cold II. A. Malan and B. Canguilhem, editors. Colloque INSERM/John Libby Eurotext Ltd., London. 347–358.

53. Wunder, B. A., and R. D. Gettinger. 1996. Effects of body mass and temperature on nonshivering thermogenic response of small mammals. *In* Adaptations to the Cold. Tenth International Hibernation Symposium. F. Geiser, A. J. Hulbert, and S. C. Nicol, editors. University of New England Press, Armidale, Australia. 131–139.

54. Cooney, G. J., I. D. Caterson, and E. A. Newsholme. 1985. The effect of insulin and noradrenaline on the uptake of 2-[1-14C]deoxyglucose in vivo by brown adipose tissue and other glucose-utilising tissues of the mouse. *FEBS Lett.* **188:** 257–261.

55. Rabi, T., Y. Cassuto, and A. Gutman. 1977. Lipolysis in brown adipose tissue of cold- and heat-acclimated hamsters. *J. Appl. Physiol.* **43:** 1007–1011.

56. Kuusela, P., J. Nedergaard, and B. Cannon. 1986. Beta-adrenergic stimulation of fatty acid release from brown fat cells differentiated in monolayer culture. *Life Sci.* **38:** 589–599.

57. Brooks, B. J., J. R. Arch, and E. A. Newsholme. 1983. Effect of some hormones on the rate of the triacylglycerol/fatty-acid substrate cycle in adipose tissue of the mouse in vivo. *Biosci. Rep.* **3:** 263–267.

58. Inokuma, K., Y. Ogura-Okamatsu, C. Toda, K. Kimura, H. Yamashita, and M. Saito. 2005. Uncoupling protein 1 is necessary for norepinephrine-induced glucose utilization in brown adipose tissue. *Diabetes.* **54:** 1385–1391.

59. Laury, M. C., M. F. Chapey, and R. Portet. 1987. Involvement of the sympathetic nervous system in lipolytic activity in brown adipose tissue of cold acclimated rats. *Comp. Biochem. Physiol. A.* **87:** 197–203.

60. Ouellet, V., S. M. Labbé, D. P. Blondin, S. Phoenix, B. Guérin, F. Haman, E. E. Turcotte, D. Richard, and A. C. Carpentier. 2012. Brown adipose tissue oxidative metabolism contributes to energy expenditure during acute cold exposure in humans. *J. Clin. Invest.* **122:** 545–552.

61. Bartelt, A., O. T. Bruns, R. Reimer, H. Hohenberg, H. Ittrich, K. Peldschus, M. G. Kaul, U. I. Tromsdorf, H. Weller, C. Waurisch, et al. 2011. Brown adipose tissue activity controls triglyceride clearance. *Nat. Med.* **17:** 200–205.

62. Klingenspor, M., S. Klaus, H. Wiesinger, and G. Heldmaier. 1989. Short photoperiod and cold activate brown fat lipoprotein lipase in the Djungarian hamster. *Am. J. Physiol.* **257:** R1123–R1127.

63. Uchida, K., T. Shiuchi, H. Inada, Y. Minokoshi, and M. Tominaga. 2010. Metabolic adaptation of mice in a cool environment. *Pflugers Arch.* **459:** 765–774.

64. Azzu, V., and M. D. Brand. 2010. The on-off switches of the mitochondrial uncoupling proteins. *Trends Biochem. Sci.* **35:** 298–307.

65. Fedorenko, A., P. V. Lishko, and Y. Kirichok. 2012. Mechanism of fatty-acid-dependent UCP1 uncoupling in brown fat mitochondria. *Cell.* **151:** 400–413.

66. Foster, D. O., and M. L. Frydman. 1978. Nonshivering thermogenesis in the rat. II. Measurements of blood flow with microspheres point to brown adipose tissue as the dominant site of the calorigenesis induced by noradrenaline. *Can. J. Physiol. Pharmacol.* **56:** 110–122.

67. Himms-Hagen, J. 1974. Interscapular location of brown adipose tissue: role in noradrenaline-induced calorigenesis in cold-acclimated rats. *Can. J. Physiol. Pharmacol.* **52:** 225–229.

68. Laury, M. C., and R. Portet. 1974. Effects of the partial removal of the brown fat and of theophylline on the calorigenic response to noradrenaline in the rat adapted to cold. *Rev. Can. Biol.* **33:** 15–25.

69. Foster, D. O., and M. L. Frydman. 1978. Brown adipose tissue: the dominant site of nonshivering thermogenesis in the rat. *Experientia Suppl.* **32:** 147–151.

70. Heldmaier, G., and A. Buchberger. 1985. Sources of heat during nonshivering thermogenesis in Djungarian hamsters: a dominant role of brown adipose tissue during cold adaptation. *J. Comp. Physiol. B.* **156:** 237–245.

71. Nedergaard, J., V. Golozoubova, A. Matthias, I. Shabalina, K. Ohba, K. Ohlson, A. Jacobsson, and B. Cannon. 2001. Life without UCP1 : mitochondrial, cellular and organismal characteristics of the UCP1-ablated mice UCP1. *Biochem. Soc. Trans.* **29:** 756–763.

72. Mineo, P. M., E. A. Cassell, M. E. Roberts, and P. J. Schaeffer. 2012. Chronic cold acclimation increases thermogenic capacity, non-shivering thermogenesis and muscle citrate synthase activity in both wild-type and brown adipose tissue deficient mice. *Comp. Biochem. Physiol. A Mol. Integr. Physiol.* **161:** 395–400.

73. Cannon, B., and J. Nedergaard. 2011. Nonshivering thermogenesis and its adequate measurement in metabolic studies. *J. Exp. Biol.* **214:** 242–253.

74. Petrovic, N., T. B. Walden, I. G. Shabalina, J. A. Timmons, B. Cannon, and J. Nedergaard. 2010. Chronic peroxisome proliferator-activated receptor gamma (PPARgamma) activation of epididymally derived white adipocyte cultures reveals a population of thermogenically competent, UCP1-containing adipocytes molecularly distinct from classic brown adipocytes. *J. Biol. Chem.* **285:** 7153–7164.

75. Vosselman, M. J., W. D. van Marken Lichtenbelt, and P. Schrauwen. 2013. Energy dissipation in brown adipose tissue: from mice to men. *Mol. Cell. Endocrinol.* **379:** 43–50.

76. Lidell, M. E., M. J. Betz, O. D. Leinhard, M. Heglind, L. Elander, M. Slawik, T. Mussack, D. Nilsson, T. Romu, P. Nuutila, et al. 2013. Evidence for two types of brown adipose tissue in humans. *Nat. Med.* **19:** 631–634.

77. Schulz, T. J., P. Huang, T. L. Huang, R. Xue, L. E. McDougall, K. L. Townsend, A. M. Cypess, Y. Mishina, E. Gussoni, and Y-H. Tseng. 2013. Brown-fat paucity due to impaired BMP signalling induces compensatory browning of white fat. *Nature.* **495:** 379–383.

78. Mezentseva, N. V, J. S. Kumaratilake, and S. A. Newman. 2008. The brown adipocyte differentiation pathway in birds: an evolutionary road not taken. *BMC Biol.* **6:** 17.

79. Flachs, P., R. Rühl, M. Hensler, P. Janovska, P. Zouhar, V. Kus, Z. Macek Jilkova, E. Papp, O. Kuda, M. Svobodova, et al. 2011. Synergistic induction of lipid catabolism and anti-inflammatory lipids in white fat of dietary obese mice in response to calorie restriction and n-3 fatty acids. *Diabetologia.* **54:** 2626–2638.

80. Flachs, P., M. Rossmeisl, O. Kuda, and J. Kopecky. 2013. Stimulation of mitochondrial oxidative capacity in white fat independent of UCP1: a key to lean phenotype. *Biochim. Biophys. Acta.* **1831:** 986–1003.

81. Garofalo, M. A., I. C. Kettelhut, J. E. Roselino, and R. H. Migliorini. 1996. Effect of acute cold exposure on norepinephrine turnover rates in rat white adipose tissue. *J. Auton. Nerv. Syst.* **60:** 206–208.

82. Lafontan, M., and D. Langin. 2009. Lipolysis and lipid mobilization in human adipose tissue. *Prog. Lipid Res.* **48:** 275–297.

83. Newsholme, E. A., and B. Crabtree. 1976. Substrate cycles in metabolic regulation and in heat generation. *Biochem. Soc. Symp.* **1976:** 61–109.

84. Nedergaard, J., T. Bengtsson, and B. Cannon. 2007. Unexpected evidence for active brown adipose tissue in adult humans. *Am. J. Physiol. Endocrinol. Metab.* **293:** E444–E452.

85. Wu, J., P. Boström, L. M. Sparks, L. Ye, J. H. Choi, A-H. Giang, M. Khandekar, K. A. Virtanen, P. Nuutila, G. Schaart, et al. 2012. Beige adipocytes are a distinct type of thermogenic fat cell in mouse and human. *Cell.* **150:** 366–376.

86. Enerbäck, S. 2010. Human brown adipose tissue. *Cell Metab.* **11:** 248–252.